

# Continuous wave cavity ring-down spectroscopy applied to *in situ* detection of dinitrogen pentoxide (N<sub>2</sub>O<sub>5</sub>)

William R. Simpson<sup>a)</sup>

Department of Chemistry and Geophysical Institute, University of Alaska Fairbanks, Fairbanks, Alaska 99775-6160

(Received 28 February 2003; accepted 17 March 2003)

We describe an instrument using cavity ring-down spectroscopy (CRDS), an ultrasensitive detection method, to detect NO<sub>3</sub> and N<sub>2</sub>O<sub>5</sub> (via thermal dissociation to NO<sub>3</sub> at 80 °C). We use continuous-wave (cw) cavity ring-down spectroscopy, allowing a highly reliable diode laser to act as the light source. This instrument uses all solid-state laser and optical components, and it is compact, portable, and power efficient. Advantages and disadvantages of cw CRDS compared to pulsed CRDS are discussed. Inlet losses and possible interferences were extensively investigated. We show field observations of N<sub>2</sub>O<sub>5</sub> mixing ratios in ambient air. Dinitrogen pentoxide was measured because low ambient temperatures shift the equilibrium between NO<sub>3</sub>, NO<sub>2</sub>, and N<sub>2</sub>O<sub>5</sub> strongly towards N<sub>2</sub>O<sub>5</sub>. Therefore, only N<sub>2</sub>O<sub>5</sub> is present in significant quantities in the Fairbanks, AK, during winter. From these data, we identify times where the N<sub>2</sub>O<sub>5</sub> mixing ratio must be zero (due to the absence of ozone indicating presence of NO) and use these time periods to measure the system's operational detection limit. The 2σ detection limit for N<sub>2</sub>O<sub>5</sub> is 2.4 parts per trillion by volume (pptv) in a 25 s average. Prediction of the N<sub>2</sub>O<sub>5</sub> detection limit from estimates of ring-down signal noise indicates a detection limit of 1.6 pptv, in the same averaging period. The observed detection limit is about 50% larger than the predicted detection limit, indicating that other noise sources affect the true detection limit. A similar instrument using pulsed CRDS was described in the last year, and we compare our instrument to this instrument for detection of N<sub>2</sub>O<sub>5</sub>. © 2003 American Institute of Physics. [DOI: 10.1063/1.1578705]

## I. INTRODUCTION

Our understanding of the chemistry of the atmosphere relies upon accurate observations of trace gas abundances. Measurements of reactive trace gases are particularly important because these gases often control the lifetime of more stable gases and modify particulate matter in the atmosphere. The nitrate radical, NO<sub>3</sub>, and its related reservoir compound, dinitrogen pentoxide, N<sub>2</sub>O<sub>5</sub>, are important intermediates in atmospheric nitrogen chemistry.<sup>1,2</sup> The nitrate radical is primarily formed by oxidation of NO<sub>x</sub> (NO+NO<sub>2</sub>) by ozone. Subsequently, nitrate radical can react with NO<sub>2</sub> to form N<sub>2</sub>O<sub>5</sub> reversibly



At typical temperatures and concentrations of NO<sub>2</sub> in the lower troposphere, the relaxation time of this equilibrium is on the order of seconds to hours. Reaction (1) is also very strongly temperature dependent, with N<sub>2</sub>O<sub>5</sub> being the dominant species at temperatures below freezing. Both NO<sub>3</sub> and N<sub>2</sub>O<sub>5</sub> are reactive in the atmosphere. The nitrate radical can initiate oxidation of organics as well as add across double bonds of unsaturated organics.<sup>1,3</sup> Dinitrogen pentoxide can react heterogeneously with water to give two molecules of nitric acid.<sup>2,4</sup> Either of these pathways presents a loss mechanism for NO<sub>x</sub> that does not require UV light. These NO<sub>x</sub> loss mechanisms are in contrast to OH oxidation of NO<sub>2</sub>, a pro-

cess that requires UV to produce OH. The nitrate radical absorbs visible light and is photolyzed by light with wavelengths shorter than about 640 nm.<sup>5</sup> Therefore, the chemistry of NO<sub>3</sub> and N<sub>2</sub>O<sub>5</sub> is only active during night. Polar regions during winter experience long nights, dim days, and low temperatures, all of which are conditions that activate NO<sub>3</sub> and N<sub>2</sub>O<sub>5</sub> chemistry. Therefore, we have built an instrument to quantify these compounds in the ambient atmosphere.

The nitrate radical has been routinely measured in the atmosphere by long-path spectroscopy,<sup>6–11</sup> while the N<sub>2</sub>O<sub>5</sub> has only been recently detected.<sup>12–14</sup> Long-path spectroscopy measures the average concentration of NO<sub>3</sub> over a path that is typically more than 5 km, therefore short-distance (and short-time scale) concentration fluctuations are not observable. For this reason, we (and others) set out to use cavity ring-down spectroscopy (CRDS) to detect NO<sub>3</sub>. Cavity ring-down spectroscopy, described below, uses high-reflectivity mirrors to achieve long effective path lengths in a short base path, allowing *in situ* detection of NO<sub>3</sub>. Additionally, by heating the sampled air, we can thermally dissociate N<sub>2</sub>O<sub>5</sub> and measure the sum of NO<sub>3</sub>+N<sub>2</sub>O<sub>5</sub>. In 2000, our group demonstrated that CRDS could detect NO<sub>3</sub> by adding N<sub>2</sub>O<sub>5</sub> to room air.<sup>15</sup> Brown, Ravishankara, and co-workers solved many of the difficult sample-handling issues and detected NO<sub>3</sub> and N<sub>2</sub>O<sub>5</sub> via pulsed CRDS.<sup>12–14</sup> Ball *et al.* constructed a unique variant of CRDS using broadband laser light to detect a full spectrum on each laser shot.<sup>16</sup>

Cavity ring-down spectroscopy is a fairly mature tech-

<sup>a)</sup>Electronic mail: wrs@ozone.gi.alaska.edu

nique that has been reviewed extensively; therefore we only briefly mention its development. An interested reader can read one of the recent reviews on the subject.<sup>17–19</sup> Cavity ring-down spectroscopy, as used for spectroscopy, was first described by O’Keefe and Deacon in 1988,<sup>20</sup> although previous measurements using optical cavities had been investigated.<sup>21</sup> Cavity ring-down spectroscopy has two major variants, depending upon whether the laser source is pulsed<sup>17–20</sup> or continuous wave (cw).<sup>17,18,22–25</sup> Pulsed laser CRDS systems have the advantage of being simpler to operate, although they can suffer increased noise due to excitation of multiple cavity modes. Additionally, pulsed laser systems are typically larger and more complex than cw diode laser sources. Continuous-wave CRDS systems have the advantage of being smaller and more power efficient, with all solid-state components. However, they have a disadvantage due to the need to match the diode laser’s output to a single mode of the cavity. Imperfect mode matching can lead to increased noise and decreased data rates for a cw CRDS system. In this article, we describe a system for the detection of NO<sub>3</sub> and N<sub>2</sub>O<sub>5</sub> based upon cw CRDS. We pay special attention to the mode matching aspects of the cw CRDS method, as they present difficulties in building a field-portable instrument. We present data of ambient N<sub>2</sub>O<sub>5</sub> mixing ratios from subarctic wintertime ambient air.

## II. EXPERIMENT

Cavity ring-down spectroscopy measures the loss rate of light within an optical cavity. Numerous articles have described the method;<sup>17–19</sup> therefore we assume that the reader is familiar with the technique. The loss of light within the cavity is first order, thus the circulating intensity is given by the equation  $I(t) = I_0 \exp(-t/\tau)$ , where  $I_0$  is the initial intensity in the cavity, and  $\tau$  is the ring-down time. The ring-down time is the fundamental measurement in CRDS and quantifies the sum of all optical losses within the cavity. To detect NO<sub>3</sub>, we need a method to separate the absorption optical loss due to NO<sub>3</sub> from other optical losses within the cavity (e.g., imperfect mirror reflection, scattering and absorption by other gases and/or particles). We use the fast reaction of NO with NO<sub>3</sub> to prepare a chemically zeroed sample of ambient air with NO<sub>3</sub> removed. The change between the ring-down time for ambient air and chemically zeroed air then quantifies the concentration of NO<sub>3</sub> within the cavity. In this section, we describe our instrument for measuring NO<sub>3</sub> and N<sub>2</sub>O<sub>5</sub>, data analysis considerations, the zeroing method, and the effect of mode matching of the cavity with the laser, which is specifically required for cw CRDS.

### A. Instrumental construction

Figure 1 shows a schematic illustration of our instrument. The system is divided into two parts, the first being the electronics box, housing all electronics and gas flow control, and the second being the sampling cell. The electronics components and computer are housed in a rugged field-portable rack mount housing (Hardigg cases). The size of this box is approximately 60 cm × 68 cm × 76 cm. The two parts are coupled with an 11-m-long umbilical connector housing gas

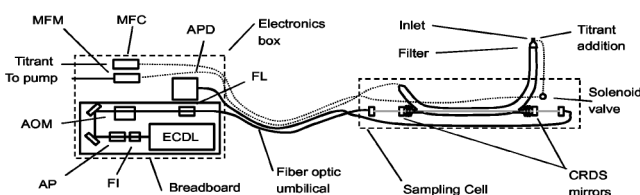


FIG. 1. Schematic layout of this instrument. The system has two major parts, the electronics box, and the sampling cell, coupled by an 11 m umbilical. Fiber-optic connections in the umbilical are labeled with solid lines, while gas tubing is shown with dotted lines.

tubing, wiring, and fiber-optic cables. With this design, the electronics box can be located in a temperature-controlled environment, while the sampling cell is located in the ambient environment.

A diode laser (ECDL in Fig. 1, EOSI model 2010) produces narrow-band ( $\sim 300$  kHz bandwidth in 50 ms) radiation near 662 nm. A Faraday isolator (FI in Fig. 1) prevents back-reflected light from entering the diode laser. Light from the diode laser is circularized with an anamorphic prism beam expander (AP in Fig. 1) then directed into an acousto-optic modulator (AOM in Fig. 1, Isomet Corporation) that acts as a fast switch. The light is then coupled into a single-mode polarization maintaining fiber-optic cable (FL in Fig. 1, Optics for Research) for transmission to the sampling cell. The diode laser and these optical components are located on a small optical breadboard (15 cm × 40 cm) that is vibration isolated from the electronics enclosure.

The laser light propagates through the fiber-optic coupling to the sampling cell enclosure (20 cm × 30 cm × 122 cm). Within the sampling cell, the CRDS optics are mounted on a set of two 1/2-in-diam steel rods that form a stable optical base. This rail system can be moved to align the CRDS axis onto the flow axis of the cell. This rail system is mounted to the cell enclosure, which is typically heated to 25 °C to minimize thermally induced optical alignment drift. The laser light emitted from the fiber optic is collimated and then directed onto a two-mirror linear cavity that is 67 cm long. The cavity mirrors (Research Electro Optics) have a reflection loss of approximately 20 ppm ( $R = 99.998\%$ ), and a transmission of 10 ppm ( $10^{-5}$ ). The mirrors are O-ring sealed to a purge chamber (described in a following section). Commercial 2 in. optical mirror mounts (Thorlabs) allow for cavity alignment. Light emitted from the cavity back mirror is focused with a 50 mm focal length lens into a 200  $\mu\text{m}$  core silica/silica multimode fiber optic that brings the light back from the umbilical to the detector, which is housed in the electronics enclosure.

The laser light returning from the cavity enclosure is measured with a silicon avalanche photodiode (APD in Fig. 1) in a detector module (Hamamatsu C5460). The signal from the detector is recorded with a 12 bit 1.25 MSa/s digitizer card (National Instruments PCI-MIO-16E-1) mounted in a rack-mount computer within the electronics enclosure. This same card logs all other signals from flow, laser power, humidity, and temperature sensors within the electronics enclosure. The ring-down data are analyzed and logged every ring-down transient with housekeeping data recorded every 50 transients (typically 2–3 s).

The air being sampled enters the inlet either directly from the atmosphere (when the sampling cell is placed outside), or through a 2 m length of 1/2 in. o.d. 3/8 in. i.d. PFA Teflon inlet extender tube. The main analysis flow cell is made of Halocarbon wax coated cylindrical glass tubing (31 mm i.d.) with a design very similar to that of Brown *et al.*<sup>12,13</sup> For the purpose of zero concentration determination, we use a titration reaction of NO<sub>3</sub> with NO to chemically remove NO<sub>3</sub> from the ambient air (discussed following). Titrant gas (NO, 30.3 ppmv, Scott Specialty Gases) is added periodically, at a flow of 15 sccm to the inlet air through a 1/8 in. o.d. Teflon tube in the center of the flow cell tube. The flow of titrant is regulated with a mass flow controller (MFC in Fig. 1, Tylan Inc.). Once diluted into the main flow, this addition leads to ~50 ppbv NO added. The titrant gas is modulated by a three-way solenoid valve placed close to the inlet addition point to minimize dead volumes and bleeding of NO into the inlet. When the system is in measurement mode, the titrant gas is brought back through the umbilical and dumped into the common system exhaust. After the NO addition point, the air is filtered with a Teflon filter (Pall Inc., Teflo 2 micron filter). The air then enters the heated section of tubing and is heated to 80 °C and aligned along the CRDS axis by two successive 45° bends. The laser light within the cavity enters the flow cell through a glass sidearm tube blown on the 45° elbow. This sidearm tube is connected to the mirror purge chamber with a polyethylene bellows (Gagne, Inc.). The mirror purge chamber is swept clean by addition of 200 sccm (total to both mirrors) of breathing-quality air. For clarity, the purge system is not shown in Fig. 1. The length of the cell that is filled with ambient air is 50 cm long. Purging of mirrors in this way maintains high reflectivity for many weeks of continual operation. After the air has been analyzed by CRDS, it is carried to the electronics enclosure in a 1/2 in. o.d. polyethylene tube. In the electronics enclosure, the air temperature, relative humidity and total flow mass (MFM in Fig. 1) are measured. The typical total flow is 8 slpm. Separate mass flow controllers in the electronics enclosure control the NO titrant flow and purge gas flow. In this configuration, the plug-flow residence time from the inlet to the beginning of the detection region is 2 s. The time to the middle of the detection region is 3 s, and the analysis is complete in 4 s.

The system total power consumption is 100–350 W, depending on heater loads and excluding the computer cathode ray tube monitor. The system operates unattended for days, only requiring user intervention for filter changes.

## B. System operation and data analysis

The system detects NO<sub>3</sub> by measuring the change in ring-down time between ambient air ( $\tau_m$ ) and chemically zeroed ambient air ( $\tau_b$ ). The fast reaction of NO with NO<sub>3</sub> is used to chemically zero the inlet air. This reaction is highly specific to NO<sub>3</sub>, as discussed subsequently. Equation (2) converts between these two ring-down time measurements and the observed NO<sub>3</sub> concentration within the analysis cell

$$[\text{NO}_3] = \frac{1}{c\sigma} \frac{L}{L_a} \left( \frac{1}{\tau_m} - \frac{1}{\tau_b} \right). \quad (2)$$

In this equation,  $c$  is the speed of light,  $\sigma$  is the absorption cross section for NO<sub>3</sub>, and  $L$  is the total cavity length, and  $L_a$  is the length of the cavity that contains NO<sub>3</sub> (i.e., is not within the purge volumes). The ratio  $L/L_a$  was confirmed by using CRDS to detect ozone's Chappius band absorption at 662.4 nm. The absolute concentration of ozone used in this experiment was measured using a commercial UV absorption instrument (Dasibi model 1008).

In the field data shown here, we detected N<sub>2</sub>O<sub>5</sub> by heating the measurement cell to 80 °C, which converts N<sub>2</sub>O<sub>5</sub> to NO<sub>3</sub>. Because the ambient temperature was low, the equilibrium between NO<sub>3</sub> and N<sub>2</sub>O<sub>5</sub> in the atmosphere was shifted heavily towards N<sub>2</sub>O<sub>5</sub> (as discussed more fully below). Therefore, we often refer to our atmospheric measurements as N<sub>2</sub>O<sub>5</sub>, while they would be the sum of NO<sub>3</sub> and N<sub>2</sub>O<sub>5</sub> in the case that the ambient temperature was higher. The absorption cross section for NO<sub>3</sub> used in this study is at 662.4 nm and is adjusted for the elevated temperature of the analysis cell (80 °C);  $\sigma = 1.70 \times 10^{-17} \text{ cm}^2 \text{ molecule}^{-1}$ . This value is based upon the temperature correction in Wayne *et al.*,<sup>1</sup> which is an average of data available at the time.<sup>26–28</sup> Temperature correction by the measurement of Yokelson *et al.*<sup>29</sup> results in a similar cross section value. This cross section is 19% smaller than the Wayne *et al.*<sup>1</sup> recommended cross section at 662.0 nm, 298 K, and 24% smaller than at standard temperature and pressure (STP) (0 °C). After calculating the NO<sub>3</sub> concentration in the cell, the NO<sub>3</sub> abundance is converted to a mixing ratio by dividing by the air concentration in the analysis cell (at 80 °C). Unfortunately, all these factors: path length, temperature dependence of the absorption cross section, and decreased air density within the cell adversely affect the analytical detection limit. The correction for pathlength is 1.34, that due to the absorption cross section compared to STP is 1.32, and that due to the decrease in density compared to STP is 1.29, overall leading to a factor of 2.2 degradation in sensitivity compared to analysis in a filled cavity at STP.

## C. Zero determination

We use the reaction of NO with NO<sub>3</sub> periodically to remove NO<sub>3</sub> chemically from the inlet air and quantify the base line ring-down time ( $\tau_b$ ). The reaction is fast; at an addition of 50 ppbv NO, the pseudo-first order lifetime of NO<sub>3</sub> is 0.04 s at 80 °C, 1 atm,<sup>30</sup> ensuring complete zeroing before any NO even reaches the analysis region of the flow cell (2 s). The reaction rate is not strongly temperature dependent;<sup>30</sup> therefore NO is an effective titrant for NO<sub>3</sub> at 50 ppbv at all reasonable temperatures.

The addition of NO is very effective in modulating the NO<sub>3</sub> concentration; however a number of other compounds react with NO and should be considered as possible interferences. In order to be an interferer, the molecule must react with NO on the time scale of the residence within the analysis cell (3 s) and must absorb light at 662.4 nm. In addition to NO<sub>3</sub>, ozone, NO<sub>2</sub>, and water vapor absorb, and particulate matter scatters and absorbs at 662.4 nm. Particulate matter is

removed on the inlet filter, and thus is not considered. Water does not react with NO; therefore is not modulated (except via dilution), leaving ozone and NO<sub>2</sub> as possible problems.

Ozone reacts with NO moderately rapidly. The pseudo-first order rate coefficient for ozone destruction at 50 ppbv NO is  $\sim 22$  s (at 80 °C). Therefore, within the measurement time of 3 s (the time for a plug flow to reach the middle of the analysis region), approximately 13% of ambient ozone is destroyed. The absorption cross section of ozone in this band is quite weak ( $\sigma = 2.0 \times 10^{-21}$  cm<sup>2</sup> molecule<sup>-1</sup>),  $\sim 10^{-4}$  of that of NO<sub>3</sub>. This cross section is from Burkholder and Talukdar (1994),<sup>31</sup> which agrees with the peak cross sections of Anderson and Mauersberger (1992).<sup>32</sup> Thus, the overall interference of ozone is  $1.2 \times 10^{-5}$  less sensitive than NO<sub>3</sub>. Therefore, 80 ppbv of ozone appear as 1 pptv of NO<sub>3</sub> if this were the only effect of ozone; however, when NO reacts with ozone, NO<sub>2</sub> is formed. NO<sub>2</sub> has a variable cross section in this region, with a value of ( $\sigma \sim 2 \times 10^{-21}$  cm<sup>2</sup> molecule<sup>-1</sup> at 662.4 nm<sup>33</sup>), approximately equal to that of ozone. This cross section depends on wavelength, so we estimate an uncertainty in the cross section of  $\pm 0.8 \times 10^{-21}$  cm<sup>2</sup> molecule<sup>-1</sup> arising from wavelength uncertainty. Because of the near equality of the NO<sub>2</sub> and ozone cross sections, the absorption caused by ozone is replaced by absorption of NO<sub>2</sub> formed by the NO+O<sub>3</sub> reaction. The complete ozone interference sensitivity is given by the difference of the ozone cross section minus that of NO<sub>2</sub>. Therefore, the NO<sub>2</sub> absorption compensates for the loss of ozone absorption through production of NO<sub>2</sub>, and the interference is  $< \pm 5 \times 10^{-6}$  of that of NO<sub>3</sub>. Therefore,  $\sim 200$  ppbv of ozone would be needed to appear as  $\pm 1$  pptv of NO<sub>3</sub>. Because ambient ozone is typically less than 200 ppbv in the troposphere, there is little ozone interference. Additionally, because ozone is often measured during a field campaign, one can correct for this small effect. Alternatively, lower addition levels of NO may be used.

Reaction of NO with NO<sub>3</sub> leads to formation of two NO<sub>2</sub> molecules; therefore zeroing NO<sub>3</sub> with NO produces twice as much NO<sub>2</sub> as there was NO<sub>3</sub> present during the measurement. This effect leads to a decrease in the effective cross section for NO<sub>3</sub> because it adds an absorption during the “zero” measurement. The magnitude of the effect is twice the ratio of the absorption cross section of NO<sub>2</sub>/NO<sub>3</sub>, or approximately a  $2 \times 10^{-4}$  fractional reduction in the NO<sub>3</sub> absorption cross section, and is therefore negligibly small.

The addition of titrant to the inlet air causes a dilution of the inlet air. In the case where the inlet air contains compounds that have significant absorbances at the detection wavelength, a small modulation of the signal results. In our system, the ratio of titrant flow to total flow is 15 sccm to 8000 sccm = 0.0019. Therefore, the signal is modulated by approximately 0.2% of the absorbance. To have a modulation appearing as 1 pptv NO<sub>3</sub>, we need 5 ppmv O<sub>3</sub>, an unreasonably high level, or 5 ppmv NO<sub>2</sub>, which is also not likely. If the laser were tuned accidentally to a strong water absorbance in the region, it is possible that there would be a modulation effect; therefore, it is important to tune away from water absorbances. For a mixing ratio of 0.02 mol H<sub>2</sub>O/mol air, the water absorbance cross section would have to be approximately  $5 \times 10^{-25}$  cm<sup>2</sup> molecule<sup>-1</sup> to cause a

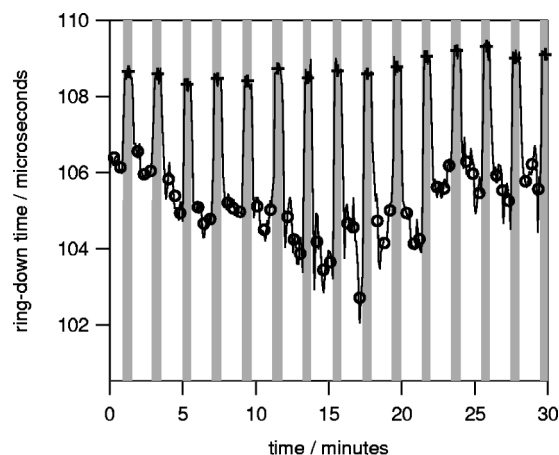


FIG. 2. Detection of N<sub>2</sub>O<sub>5</sub> in ambient Fairbanks air using cavity ring-down spectroscopy demonstrating chemical zeroing with NO. N<sub>2</sub>O<sub>5</sub> is detected by conversion to NO<sub>3</sub> in a heated detection cell (80 °C) followed by CRDS measurement of NO<sub>3</sub>. The solid line shows 5 s averages of the ring-down time measured at 662.4 nm as a function of time. During the times with shaded background, the cavity's background is measured by adding NO to the inlet, removing all NO<sub>3</sub>. During the times with a white background, ambient air is sampled, and the NO<sub>3</sub>'s optical absorption at this wavelength increases the cavity loss, decreasing the ring-down time. The crosses are 25 s measurements of the base line ring-down time, while open circles are 25 s measurements of the ambient air ring-down time.

dilution-induced modulation that appears as 1 pptv NO<sub>3</sub>. This cross section is near the peaks of the water lines in this spectral region. If the laser were tuned to a water absorption feature of this strength, the base line ring-down time would clearly be affected; therefore this effect is fairly easily avoided.

Another possible interference due to zeroing involves pressure or temperature variations. Cavity ring-down spectroscopy measures the total optical extinction in the cavity, and thus Rayleigh scattering affects the ring-down time. Rayleigh scattering depends on the density and index of refraction of the medium in the cavity. At 662.4 nm, 1 atm, 298 K, the scattering coefficient by pure dry air is  $b_{sg} = 5.3 \times 10^{-8}$  cm<sup>-1</sup>,<sup>34</sup> indicating that 17% of our base line ring-down time is caused by Rayleigh scattering. Therefore, air density variation of approximately 0.5% would appear as 1 pptv of NO<sub>3</sub>. This level of density change is caused by a 4 Torr of pressure variation, or a 2 K temperature variation. Because the zeroing addition is kept to 0.2% of the total flow, the zeroing-induced pressure and temperature variations are much smaller than these levels. To our knowledge, these molecules and effects are the only interferences; therefore the NO titration method should be free of uncorrectable interference at the 1 pptv NO<sub>3</sub> level.

We operate the instrument on a 2 min modulation pattern consisting of 30 s of zero measurement (NO added) followed by 90 s of ambient air measurement. The first 5 s of the zero measurement are discarded to allow NO to fill the cell; then 25 s of data are averaged. Because flushing of the NO requires more time, the first 15 s of the measurement cycle are discarded then three successive 25 s measurements of NO<sub>3</sub> are recorded.

Figure 2 demonstrates the zero determination method. As discussed below, these data are field observations of

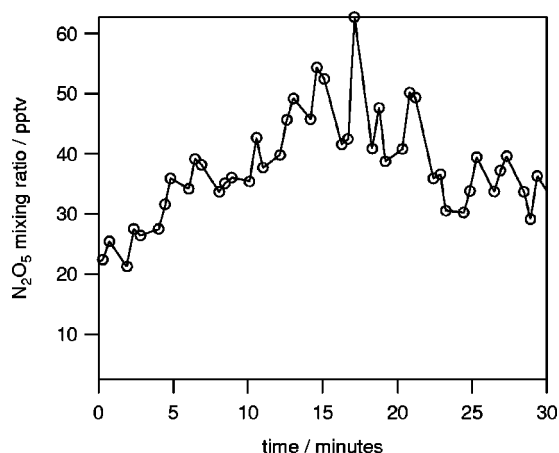


FIG. 3. Measurements of  $N_2O_5$  in ambient Fairbanks air derived from the data of Fig. 2.

$N_2O_5$  in ambient Fairbanks air, where the  $N_2O_5$  has been converted to  $NO_3$  by heating to  $80^\circ C$ . In this figure, 5 s averages of the ring-down time are shown versus real time. A 2 min modulation pattern is shown by the times with shaded background representing sampling with addition of NO and nonshaded backgrounds representing ambient air sampling. In periods where NO is added to the inlet, the base line ring-down time is measured. We quantify this base line value by averaging the 25 s of valid background data. These background ring-down times are shown as crosses. During the measurement periods, the ring-down time is reduced by the additional optical loss of  $NO_3$ 's absorption. After waiting for titrant to flush from the cavity, we use 25 s averages to quantify the measurement ring-down time, as represented by the three open circles per modulation period in the figure. The change in ring-down time between measurement and base line is used to quantify the  $NO_3$  (and  $N_2O_5$ ) concentration in the analysis cell via Eq. (2). Figure 3 shows the  $N_2O_5$  mixing ratio derived from these measurements.

#### D. Mode matching

The cw CRDS system operates differently from a pulsed CRDS system in that energy must be built up within the cavity in order to achieve a measurable ring-down signal. Because the cavity is a very high-finesse etalon, buildup can only occur when the laser is matched in frequency to one of the modes of the cavity. For a perfectly aligned cavity, the laser would be coupled to only one transverse mode of the cavity. This alignment is desirable because other transverse modes have different mirror losses (and thus a different base line ring-down time). We are mostly able to suppress other transverse modes of the cavity through alignment, but thermal drift (and possibly thermal gradients within the air in the cavity) eventually degrades the alignment. Therefore, we use two methods to suppress the influence of other transverse modes. First, we lock the laser frequency to one cavity mode, and second, we apply an outlier rejection algorithm to remove data recorded on other modes.

We achieve mode matching by tuning the laser frequency using a voltage-controlled piezoelectric transducer (PZT) within the diode laser. This sinusoidal modulation (at

50 Hz) scans the laser frequency across one of the cavity modes. A locking circuit measures the PZT voltage where the last buildup event occurred and feeds this voltage back as the center voltage for the sinusoidal modulation. Typically, the system achieves ring-down events at  $>20$  Hz. Because the circuit sometimes loses this locked state, the system actively seeks a new lock if no buildup events are found within the last second. Because the depth of modulation of the scan is only 20% of a free spectral range, other transverse modes are selected against, improving the performance of the system.

The ring-down time of each individual event is recorded for later analysis. In this later analysis, 25 s of data are considered as a data set. The mean of this data set is calculated, then all data outside a band of  $\pm 2.5\%$  of the original mean are discarded as possible excitation of other modes. The typical standard deviation of the ring-down time is 1% ( $1\sigma$ ) when the system is operating on one single transverse mode at  $80^\circ C$ . Therefore, a range of  $\pm 2.5\sigma$  should encompass  $>95\%$  of the valid data. After this data trimming, the mean of the remaining data is recorded as the mean ring-down time for the 25 s period. For our system operating continuously over an 11-day period,  $>93\%$  of the data were within the valid data type. If the 25 s period had  $<50\%$  valid data, no data were reported for this measurement interval. This secondary trimming removed  $<1\%$  of the measurements over the same 11-day period.

The combination of this mode locking and data trimming allows us to determine the ring-down time over 25 s periods with enhanced noise rejection. Chemical modulation then allows determination of nitrate radical concentrations through Eq. (2). The resulting absolute concentration of  $NO_3$  is determined inside the CRDS cavity; therefore possible inlet losses need to be considered to determine ambient mixing ratios.

### III. LABORATORY TESTING

The system described here has been extensively tested to quantify inlet losses for the system. All inlet losses are  $<5\%$  in the configuration shown here; therefore the concentrations calculated from Eq. (2) represent ambient mixing ratios for Fairbanks air. These results are in agreement with those of Brown *et al.*,<sup>12-14</sup> which is not surprising, as our flow system is similar to their design. However, these tests were carried out to confirm quantitative performance of this instrument.

#### A. $NO_3$ surface loss in main flow tube

We used a movable injector system to investigate wall losses of  $NO_3$  on the halocarbon-wax coated sampling cell. In these experiments,  $NO_3$  was generated by flash heating of previously synthesized  $N_2O_5$ . The  $N_2O_5$  was delivered from a trap submerged in an acetone slush bath ( $T_f = -96^\circ C$ , 177 K) by passing a flow of ultrahigh purity (UHP)  $N_2$ , at 0.05–0.12 slpm, over the solid  $N_2O_5$ . The solid  $N_2O_5$  was synthesized by the method of Canosa-Mas *et al.*,<sup>35</sup> which is a modification of Davidson *et al.*<sup>36</sup> This flow was then heated to  $80^\circ C$  in a PFA Teflon tube to dissociate  $N_2O_5$  and then diluted with UHP  $N_2$  to a total flow rate of 5.6 slpm. At low concentrations of  $NO_2$ , calculation indicates that the recom-

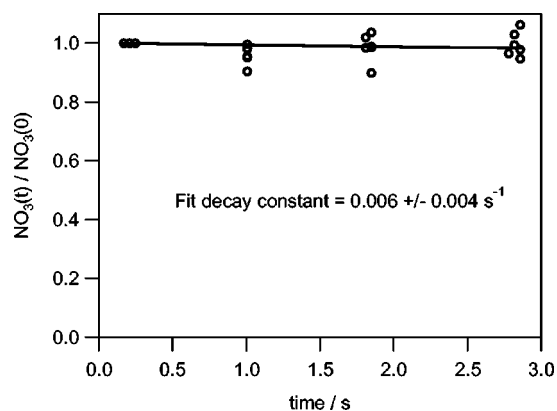


FIG. 4. Movable injector investigation of  $\text{NO}_3$  surface losses on halocarbon-wax coated tubing. The time axis represents the plug-flow residence time within 31 mm i.d. coated Pyrex tubing.

bination reaction of  $\text{NO}_2 + \text{NO}_3$  is sufficiently slow to have a stable sample of  $\text{NO}_3$  for tens of seconds. We then injected this  $\text{NO}_3$  into a halocarbon-wax coated flow tube of the same size as the main analysis tube of our instrument using a 1/4 in. o.d. Pyrex glass tube. The tube was moved over a length of 50 cm, corresponding to a plug-flow residence time variation of  $\sim 3$  s. Because the source of  $\text{NO}_3$  is not very stable, we repetitively measured the  $\text{NO}_3$  concentration at the shortest residence time and measured all concentrations relative to this shortest residence time level. The actual concentrations of  $\text{NO}_3$  varied between  $1.5 \times 10^9$  and  $3.7 \times 10^9$  molecule  $\text{cm}^{-3}$ . Figure 4 shows the result of the  $\text{NO}_3$  movable injector study. The analyzed first order rate coefficient for  $\text{NO}_3$  loss on the walls is  $0.006 \text{ s}^{-1} \pm 0.004 \text{ s}^{-1}$  ( $\pm 1\sigma$ ). Therefore, in the time for  $\text{NO}_3$  to flow to the middle of the analysis region (3 s), the transmission is 98%. Even for a worst-case scenario (mean +  $2\sigma$ )  $< 5\%$  is lost.

## B. Conversion of $\text{N}_2\text{O}_5$ to $\text{NO}_3$

To detect  $\text{N}_2\text{O}_5$ , we heated the inlet and detection regions of the flow cell to  $80^\circ\text{C}$ . At this temperature, both the rate of dissociation is sufficiently rapid and the equilibrium constant is sufficiently favorable for dissociated  $\text{NO}_3$  to not recombine with  $\text{NO}_2$ . To verify complete dissociation at  $80^\circ\text{C}$ , we measured the relative amount of  $\text{NO}_3$  detected from a  $\text{N}_2\text{O}_5$  source as a function of cell temperature. These data are shown in Fig. 5, where the error bars represent  $\pm 1\sigma$ . The relative  $\text{NO}_3$  mixing ratios are relative to the mixing ratio at  $80^\circ\text{C}$ , and are corrected for the air density variation with temperature and the temperature dependence of the absorption cross section, both discussed previously. One can clearly see a plateau in the amount of  $\text{NO}_3$  detected at temperatures above  $70^\circ\text{C}$ ; therefore, for this sample, a temperature of  $70^\circ\text{C}$  would be sufficient to detect all  $\text{N}_2\text{O}_5 + \text{NO}_3$  as  $\text{NO}_3$ . However, this source produces equimolar  $\text{NO}_3$  and  $\text{NO}_2$ , while the ambient atmosphere typically is significantly more  $\text{NO}_2$  than  $\text{NO}_3$ . The presence of excess  $\text{NO}_2$  decreases the degree of decomposition of  $\text{N}_2\text{O}_5$ , diminishing the amount of  $\text{NO}_3$  formed and detected. Therefore, we elevated the temperature to  $80^\circ\text{C}$  to ensure that all  $\text{N}_2\text{O}_5$  is detected. Calculations based upon the temperature dependent equilib-

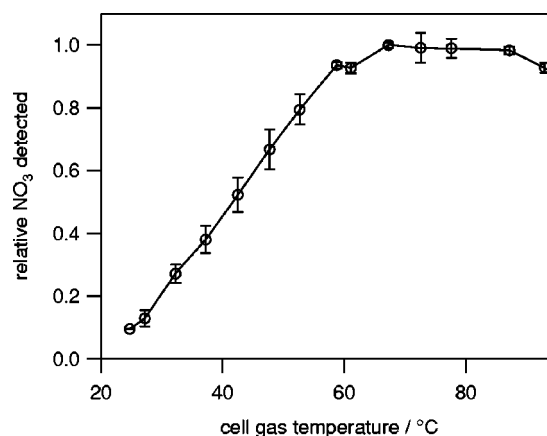


FIG. 5. The relative amount of  $\text{NO}_3$  (compared to  $80^\circ\text{C}$ ) detected from thermal dissociation of  $\text{N}_2\text{O}_5$  as a function of dissociation temperature. Error bars are  $\pm 1\sigma$ .

rium constant from DeMore *et al.*<sup>30</sup> for reaction (1) indicate that up to a mixing ratio of 20 ppbv of  $\text{NO}_2$ ,  $> 95\%$  of  $\text{N}_2\text{O}_5$  is dissociated to  $\text{NO}_3$  at  $80^\circ\text{C}$ . For detection of  $\text{N}_2\text{O}_5$  in a more polluted environment, one could heat higher or measure  $\text{NO}_2$  and correct for its effect. Because we are clearly in the plateau region, we assume 100% conversion of  $\text{N}_2\text{O}_5$  to  $\text{NO}_3$ .

## C. $\text{N}_2\text{O}_5$ loss on Teflon inlet extender tube

The field data used to test the instrument in this article were recorded using a 1/2 in. o.d., 3/8 in. i.d. PFA Teflon tube inlet extender. To investigate for possible inlet losses on this tube's surface, we undertook a second movable injector study. In this case, we are not concerned with the loss of  $\text{NO}_3$ , but the loss of  $\text{N}_2\text{O}_5$  because the inlet air is sufficiently cold to have almost all  $\text{NO}_3 + \text{N}_2\text{O}_5$  present as  $\text{N}_2\text{O}_5$ . Because  $\text{N}_2\text{O}_5$  is known to hydrolyze on surfaces, we were also concerned with the humidity of the sampled air. Therefore, we performed this test using ambient laboratory air, which contained 0.005 bars of water vapor. All field observations reported in this publication had less than this testing absolute humidity (typically much less because of low ambient temperatures).

A vapor pressure of  $\text{N}_2\text{O}_5$  is generated by flowing UHP  $\text{N}_2$  over solid  $\text{N}_2\text{O}_5$  held in a trap at acetone slush temperature ( $-96^\circ\text{C}$ ). This  $\text{N}_2\text{O}_5$  source is delivered to the instrument in a 1/8 in. o.d. PFA Teflon tube that is inserted into the 1/2 in. o.d. sampling inlet extender tube. Upon exiting the 1/8 in. o.d. inner tube, the  $\text{N}_2\text{O}_5$  flow is diluted into  $\sim 8$  slpm of ambient room air flowing in the 1/2 in. o.d. sampling tube. By varying the length of insertion of the smaller tube into the larger sampling inlet extender, we can vary the contact time of  $\text{N}_2\text{O}_5$  with the walls of the inlet extender tube. During these measurements, we periodically repeated the  $\text{N}_2\text{O}_5$  measurement at shortest contact time as a reference value. Actual mixing ratios of  $\text{N}_2\text{O}_5$  varied between 40 and 300 pptv (in separate experiments). No concentration dependence was observed. Figure 6 shows the result of these studies. The relative amount of  $\text{N}_2\text{O}_5$ , compared to the shortest contact time, is plotted against the plug-flow contact time. The error bars

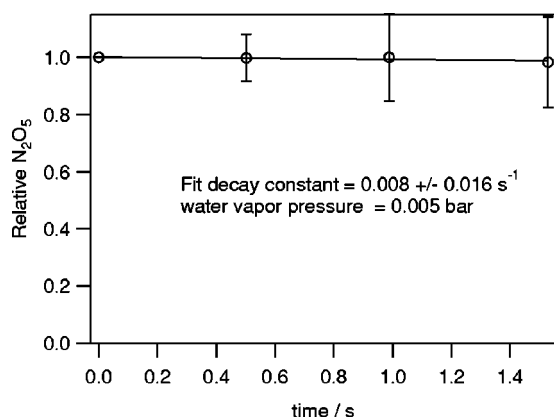


FIG. 6. Relative  $\text{N}_2\text{O}_5$  (compared to zero residence time) as a function of plug-flow residence time in the 3/8 in. i.d. PFA Teflon inlet extender tube. The error bars are  $\pm 1\sigma$ , and are large because this test was carried out using laboratory air with an absolute humidity of 0.005 bars.

on the plot are  $\pm 1\sigma$ . Some of the variability of the data points probably arises from the fact that ambient air may have compounds that react with  $\text{N}_2\text{O}_5$  (or  $\text{NO}_3$  once the air is heated). To guard partially against reactive species in the inlet air, we also operated a commercial ozone analyzer (Dasibi Model 1008-RS) and performed the experiment in the dark. When this analyzer showed nonzero ozone concentrations, we were ensured that ozone was present to react with  $\text{NO}$  that may be in the laboratory air, and the dark condition prevented photolysis of  $\text{NO}_2$  to  $\text{NO}$ . With these precautions, all but the freshest pollution will have little  $\text{NO}$ .

The analyzed loss rate for  $\text{N}_2\text{O}_5$  on this Teflon tube is  $0.008 \text{ s}^{-1} \pm 0.016 \text{ s}^{-1}$  ( $1\sigma$ ). Using the mean inlet loss in the 1.1 s residence time of the inlet indicates 99% transmission for  $\text{N}_2\text{O}_5$ . The maximum loss rate of  $\text{N}_2\text{O}_5$  on the inlet (mean plus  $2\sigma$ ) is  $0.04 \text{ s}^{-1}$ , corresponding to a maximum inlet loss of 5% in the 1.1 s residence time in the inlet tube extender. Therefore, the inlet loss of  $\text{N}_2\text{O}_5$  is  $<5\%$  for this configuration. We have not tested for  $\text{NO}_3$  loss on this inlet tube, but expect that it would be unacceptable; therefore, the inlet tube extender should only be used when the instrument is operated in  $\text{N}_2\text{O}_5$  mode, and the humidity is  $<0.005$  bars of water vapor.

#### D. Filter transmission of $\text{N}_2\text{O}_5$

A filter was used to eliminate particulate matter in the air stream to be analyzed. This filter can possibly be a source of error in measurement of  $\text{N}_2\text{O}_5$  or  $\text{NO}_3$  in the case where the filter or particulate matter accumulated on the filter is reactive to the molecule being detected. Brown *et al.*<sup>12-14</sup> tested the transmission of these filters and found that some  $\text{NO}_3$  ( $\sim 20\%$ ) is lost on the inlet filter, while  $>98\%$  of  $\text{N}_2\text{O}_5$  passes the filter. Because we are detecting these compounds in cold air, the equilibrium between  $\text{NO}_3$  and  $\text{N}_2\text{O}_5$  lies heavily towards  $\text{N}_2\text{O}_5$ , and we are concerned with the transmission of  $\text{N}_2\text{O}_5$  through the filter. We tested this transmission by generating a source of  $\text{N}_2\text{O}_5$  in UHP nitrogen. The source had a flow rate of  $\sim 0.06$  slpm and picked up a vapor pressure of  $\text{N}_2\text{O}_5$  from a trap immersed in acetone slush ( $T$

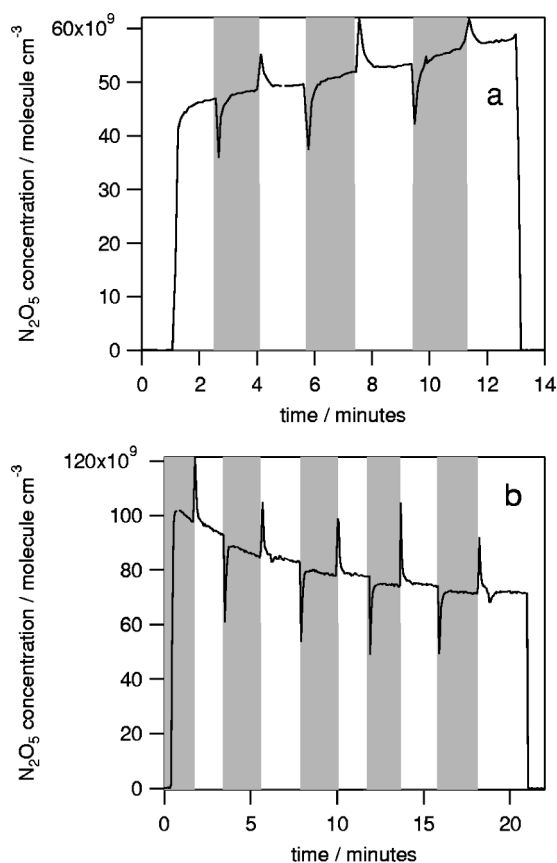


FIG. 7. Filter transmission of  $\text{N}_2\text{O}_5$  through clean (a) and loaded (b) Teflon filters. Each measurement begins and ends with a zero determination, and shaded times represent  $\text{N}_2\text{O}_5$  passing through the filter while unshaded times represent  $\text{N}_2\text{O}_5$  added after the filter (no loss reference). Transient up and down spikes immediately following switching  $\text{N}_2\text{O}_5$  addition location are artifacts and should be ignored. The filter transmission of the clean filter (a) is  $>99\%$ , and the transmission of the 46 h loaded filter (b) is  $>97\%$ .

$= -96^\circ\text{C}$ ). We then added this source to the main flow of 8 slpm UHP nitrogen either before the filter or at a secondary addition point immediately after the filter.

When adding  $\text{N}_2\text{O}_5$  after the filter,  $\text{NO}_3$  signal variability was observed. The cause of this variability is poor mixing of the small  $\text{N}_2\text{O}_5$  flow into the main flow, which is reestablishing laminar flow after passing through the filter. We eliminated this variability by adding a 1/2-in.-diam orifice (made of Teflon) downstream of the secondary addition point and adding 12 in. length of coated flow tube. The orifice caused turbulence to mix the air stream, and the secondary flow tube allowed reestablishment of laminar flow. The system was tested by measuring the difference between  $\text{N}_2\text{O}_5$  detected with sample addition in the pre- and postfilter ports but with a filter missing. There was no difference in this configuration, indicating that mixing was sufficient.

Figure 7 panel (a) shows the result of a test of the filter transmission through a new filter. The times shown as shaded have the  $\text{N}_2\text{O}_5$  added before the filter, and thus are passing the  $\text{N}_2\text{O}_5$  through the filter. Unshaded times represent periods where the  $\text{N}_2\text{O}_5$  is added after the filter. The transmission of the clean filter is  $>99\%$ . Because the particulate matter collected on the filter may be reactive to  $\text{N}_2\text{O}_5$ , we also tested highly loaded filters. In Fig. 7 panel (b), we show a

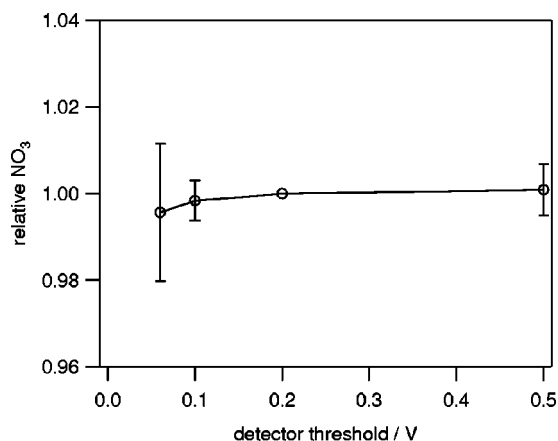


FIG. 8. Test for optical saturation of the NO<sub>3</sub> absorption. The relative NO<sub>3</sub> signal (compared to that at 0.2 V threshold) is plotted against the threshold voltage. Higher threshold voltages correspond to higher optical powers in the cavity.

transmission test on a filter that was loaded for 46 h (at 8 slpm, a total loading volume of 22 m<sup>3</sup>). This filter was clearly brown in appearance, indicating significant loading of particles. In the panel, we can see that some N<sub>2</sub>O<sub>5</sub> is lost on the filter, but the transmission is still >97%. Because particulate matter concentrations are very variable, we changed filters on a more frequent schedule; typically a filter was used for 6–12 h. In the future, we hope to analyze the particulate matter trapped on the filter to gain understanding of the role of particulates in catalyzing destruction of N<sub>2</sub>O<sub>5</sub> in the ambient atmosphere.

### E. Optical saturation test

High optical fluences can cause saturation, altering the relationship between concentration and absorption. In the case of NO<sub>3</sub> detection using CRDS, a simple calculation of the number of photons absorbed by each NO<sub>3</sub> molecule indicates that there probably is not a problem with optical saturation. However, we can perform an experimental test for saturation by varying the threshold energy where we initiate the CRDS transient. This threshold energy is  $I_0$  at the start of the ring-down transient. For our system, the transmission of a single mirror is approximately  $10^{-5}$ , and the detector sensitivity is  $10^6$  V / W. Therefore, the threshold running power within the cavity is 0.1 W / V. Typically, we use a threshold voltage to trigger the ring-down transient of 0.3 V, corresponding to 30 mW running power in the cavity at the start of the ring-down transient.

To test for possible saturation, we recorded the relative NO<sub>3</sub> signal as a function of threshold voltage. The result of this study is shown in Fig. 8. The NO<sub>3</sub> concentration relative to the NO<sub>3</sub> concentration detected at 0.2 V threshold is plotted against the threshold voltage. If saturation were occurring, higher relative NO<sub>3</sub> levels would be detected at lower thresholds, which is not the case. Therefore, optical saturation is not a problem for NO<sub>3</sub> in our system with threshold running powers up to at least 50 mW.

### F. Summary of laboratory-derived correction factors

Our detection calibration relies on the absolute calibration of the absorption sensitivity in CRDS in addition to quantification of inlet losses and physical effects (e.g., path length reduction). We have confirmed quantitative operation of our cw CRDS method using the known water vapor absorbance in this spectral region.<sup>22</sup> By far, the majority of our correction factors arise from physical effects. Using our purge geometry requires a correction for path length reduction (1.34). This effect would be the same for either NO<sub>3</sub> or N<sub>2</sub>O<sub>5</sub> detection. For detection of N<sub>2</sub>O<sub>5</sub>, we heat the inlet, leading to the temperature-dependent absorption cross section reduction compared to STP (1.32), and the density reduction compared to STP (1.29). In addition to these physical effects, inlet losses compromise a small loss for N<sub>2</sub>O<sub>5</sub>. The transmission of NO<sub>3</sub> on the halocarbon-wax coated surfaces 98%. The conversion of N<sub>2</sub>O<sub>5</sub> to NO<sub>3</sub> is 100%. The inlet tube extender (if used) transmits 99% of N<sub>2</sub>O<sub>5</sub>. And the filter transmits 99% of N<sub>2</sub>O<sub>5</sub>, possibly down to 97% with large aerosol loadings. The zeroing efficiency is assumed to be 100%. Overall, the inlet loss correction factor is 1.04 for N<sub>2</sub>O<sub>5</sub> using fresh filters and with the inlet extender. Therefore, the overall correction factor for N<sub>2</sub>O<sub>5</sub> is 2.4 compared to a filled cavity at STP. To estimate sensitivity to NO<sub>3</sub> at STP, we consider the path length correction in addition to the loss for NO<sub>3</sub> transmission and assume 80% filter transmission.<sup>13</sup> Thus the estimated overall correction factor for NO<sub>3</sub> at STP compared to a loss-free filled cell at STP is 1.7.

### IV. FIELD OBSERVATIONS

We used this system to measure N<sub>2</sub>O<sub>5</sub> mixing ratios over an 11-day period in late December 2002–January 2003. The measurements were made by sampling ambient air with a 1/2 in. o.d. PFA Teflon inlet extender fed through a gas-sampling port in the wall of the International Arctic Research Center (IARC) building on the University of Alaska Fairbanks (UAF) campus. This location is on the northwestern edge of the city of Fairbanks. The gas-sampling port is on the third floor of this four-story building, facing north, away from the city of Fairbanks. The sampling tube protruded approximately 75 cm from the building surface, which is primarily glass. Temperatures were always below freezing (the highest daily average temperature was  $-10^{\circ}\text{C}$ ), therefore equilibrium between NO<sub>2</sub>, NO<sub>3</sub> and N<sub>2</sub>O<sub>5</sub> (reaction 1) always highly favored N<sub>2</sub>O<sub>5</sub>. This equilibrium also responds to the concentration of NO<sub>2</sub>, and for very low concentrations of NO<sub>2</sub>, it is possible that N<sub>2</sub>O<sub>5</sub> would be driven to thermally dissociate. At a mixing ratio of 200 pptv NO<sub>2</sub>, and for a temperature of  $-10^{\circ}\text{C}$  at 1 atm, more than 95% of the sum of N<sub>2</sub>O<sub>5</sub>+NO<sub>3</sub> is present as N<sub>2</sub>O<sub>5</sub>. Because the temperature was typically below  $-10^{\circ}\text{C}$ , and the air masses detected were nearly certainly more polluted than 200 pptv NO<sub>2</sub>, we feel the assumption that nearly all of our signal arises from N<sub>2</sub>O<sub>5</sub> in the ambient atmosphere, with very low levels of NO<sub>3</sub>. The reason we pick this minimum NO<sub>2</sub> abundance is that Beine *et al.* measured NO<sub>x</sub> mixing ratios at Poker Flat (~50 km NE of Fairbanks) and observed a mean mixing

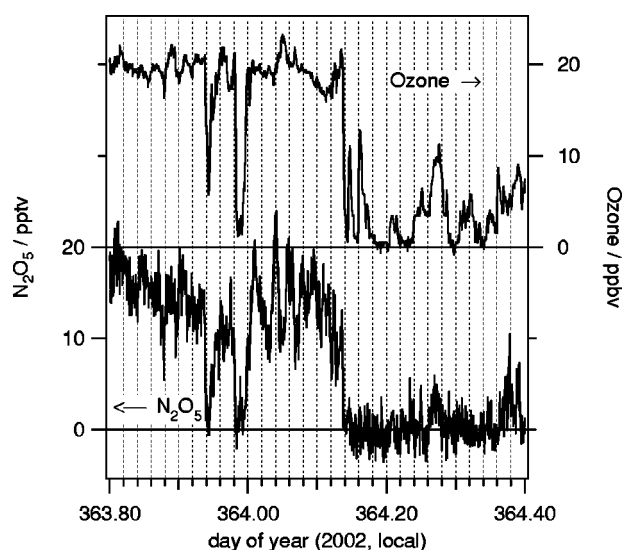


FIG. 9. Ambient ozone and  $\text{N}_2\text{O}_5$  mixing ratios from near midnight on 29–30 Dec. 2002. Ozone mixing ratios read on the right hand axis, in ppbv, and  $\text{N}_2\text{O}_5$  mixing ratios read on the left axis, in pptv. The two signals are offset vertically for clarity.

ratio of  $\sim 290$  pptv;<sup>37,38</sup> therefore, levels below 200 pptv  $\text{NO}_2$  are unlikely near Fairbanks (the dominant pollution source for Poker Flat). For these reasons, the instrument was only run in the  $\text{N}_2\text{O}_5$  detection mode (i.e., with heated inlet and cell), and the observed data are reported as  $\text{N}_2\text{O}_5$ .

### A. Behavior of $\text{N}_2\text{O}_5$ with respect to ozone

A portion of the campaign's data is shown in Fig. 9. In the bottom time series is that of  $\text{N}_2\text{O}_5$ , while the top is ozone. Ozone and  $\text{N}_2\text{O}_5$  are positively correlated during this time period. Part of the reason for this correlation is that ozone is acting as an indicator of NO in the air being sampled. Ozone reacts with NO, forming  $\text{NO}_2$  and oxygen; therefore, when ozone is present, it reacts rapidly with NO, destroying the NO. If the photolysis rate of  $\text{NO}_2$  is low enough, then the NO will decrease to near-zero levels. In the data shown in Fig. 9, the sun is always below the horizon due to the short day length in Fairbanks winter. Therefore, presence of ozone indicates the absence of NO for these nighttime data. However, if the ozone is depleted to zero, NO can remain in the atmosphere. Therefore, the absence of ozone is likely to indicate the presence of NO, and NO reacts rapidly with  $\text{NO}_3$ , removing  $\text{NO}_3$  from the atmosphere. As  $\text{NO}_3$  is removed,  $\text{N}_2\text{O}_5$  thermally dissociates, and  $\text{N}_2\text{O}_5$  soon disappears. In fact, even if  $\text{N}_2\text{O}_5$  were kinetically stable in the ambient atmosphere in the presence of NO (which is the case to some degree at low temperatures), the detection method we use would be unable to detect the metastable  $\text{N}_2\text{O}_5$ . The heating of the inlet air to dissociate  $\text{N}_2\text{O}_5$  is the cause of this artifact. Heating dissociates any  $\text{N}_2\text{O}_5$  present to  $\text{NO}_3$ , which then reacts with the NO co-pollutant in the sampled ambient air. Therefore, at any time where NO is present, our instrument is incapable of correctly quantifying any transiently stable  $\text{N}_2\text{O}_5$ . At very cold temperatures, this effect could be an issue because the thermal lifetime of  $\text{N}_2\text{O}_5$  can be hours.

This NO effect is visible in the correlated negative

spikes in ozone and  $\text{N}_2\text{O}_5$  at day of year 363.94 and 363.98. Finally, the large influx of polluted air at day of year 364.14 destroys nearly all  $\text{N}_2\text{O}_5$  signal. We can use the fact that  $\text{N}_2\text{O}_5$  must be zero when NO is present to measure the actual system's performance, as described in the next section.

### B. Calculated and actual system performance

System performance can be estimated by a calculation derived from the variability of the ring-down time or by actual measurements during times when atmospheric NO is present, guaranteeing that no  $\text{NO}_3$  or  $\text{N}_2\text{O}_5$  is present. The former method underestimates the actual noise on the system because zero drift is not included in the calculation.

Using the former method, the shot-to-shot noise of our system when operating on a single mode is 1% at 80 °C, therefore, 400 ring-down times (typical for 25 s) give a noise of 0.05%, around a base line ring-down time of 110  $\mu\text{s}$ . Therefore, the  $1\sigma$  noise of our 25 s measurement is calculated to be  $1.5 \times 10^{-10} \text{ cm}^{-1}$ . Because we use zeroing, one would predict a noise on the difference of two successive measurements to be  $\sqrt{2}$  times larger. Conversion to a detection limit for  $\text{NO}_3$  at STP, including path length reduction and surface losses, gives a  $2\sigma$  calculated noise of 1.2 pptv in the 25 s average (using the 1% system noise characteristic of 80 °C). Actual ring-down noise at ambient temperature is smaller, possibly indicating thermally induced mode fluctuations are present in the heated cell. Detection of  $\text{N}_2\text{O}_5$  has a higher detection limit, because analysis is carried out at higher temperature, where both the air density and absorption cross section are lower. The calculated detection limit for  $\text{N}_2\text{O}_5$  ( $2\sigma$ ) is 1.6 pptv in this 25 s interval.

Another method for detection limit determination uses the noise on observed data during periods where the analyte is absent to quantify system noise. This method takes into consideration zero drift and any other noise sources. We selected approximately 12 h of data during periods where ozone was zero at our monitoring site, indicating that excess NO was present in the polluted air mass, precluding detection of significant  $\text{NO}_3$  and  $\text{N}_2\text{O}_5$ . A histogram of the  $\text{N}_2\text{O}_5$  data during this time is shown in Fig. 10. The data have a standard deviation of 1.2 pptv, and a mean of  $-0.13$  pptv. We used a  $\chi^2$  test to show that, at the 95% confidence level, the data shown are statistically indistinguishable from a Gaussian distribution (shown as a solid curve in Fig. 10). The standard error (standard deviation divided by the square root of the number of observations) is 0.04 pptv, indicating that the mean of the data is approximately three standard errors different from zero. Therefore, it appears that there is a small bias present in these selected data. We cannot explain this apparent small bias. Considerations of known interferences, described previously, cannot explain this bias without unreasonably large mixing ratios of possible interferers. Possibly pressure or temperature variation during zeroing is responsible for this small bias. We do note that the bias is an order of magnitude smaller than the  $1\sigma$  error on a 25 s measurement.

From the data in Fig. 10, the  $2\sigma$  detection limit is 2.4 pptv for  $\text{N}_2\text{O}_5$  in a 25 s average. A corresponding detection

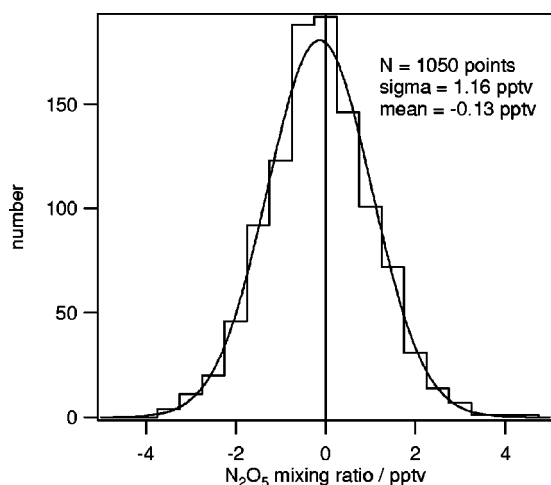


FIG. 10. A histogram of 1050 measurements of  $\text{N}_2\text{O}_5$  during times where ozone was absent in the atmosphere, indicating excess NO was present and precluding significant levels of  $\text{N}_2\text{O}_5$ . This histogram represents the noise on our measurement of  $\text{N}_2\text{O}_5$ , and leads to a  $2\sigma$  detection limit of 2.4 pptv in a 25 s measurement period.

limit for  $\text{NO}_3$  at STP would be 1.7 pptv. These actual detection limits are approximately 50% larger than those estimated from the variability of the ring-down time, indicating that zero drift, and possibly other instrumental noise sources contribute to the actual instrumental noise. We consider the second, more conservative, method better and the proper estimate of system noise.

## V. DISCUSSION

The instrument described in this article detects  $\text{NO}_3$  and  $\text{N}_2\text{O}_5$  at ambient atmospheric levels with calibration via a combination of absolute absorption spectroscopy and extensive testing and elimination of inlet losses. The instrument is similar to that of Brown *et al.*,<sup>12–14</sup> with a number of differences, described below. Our findings of no significant surface losses for  $\text{NO}_3/\text{N}_2\text{O}_5$  are in agreement with those of Brown *et al.* and confirm that the techniques described here are applicable for detection of these compounds in ambient atmospheres.

Because our testing was carried out in the winter, our system was operated in a heated mode to detect  $\text{N}_2\text{O}_5 + \text{NO}_3$ . We have argued that most of the reservoir of  $\text{NO}_3 + \text{N}_2\text{O}_5$  is in the form of  $\text{N}_2\text{O}_5$  due to the cold temperatures, and likely moderate to high  $\text{NO}_2$  present in the air sampled. Therefore, we focused on inlet losses of  $\text{N}_2\text{O}_5$ . We found that Teflon filters were capable of transmitting  $>99\%$  of  $\text{N}_2\text{O}_5$ , and that the collection of aerosol on the filter is not a problem for fairly long periods of time (46 h). However, as aerosol mass loadings in the atmosphere are highly variable in time and space, more frequent filter changes were used and are recommended. The filter lifetimes of Brown *et al.* (1 h)<sup>13</sup> are significantly shorter. The fact that their filter must transmit  $\text{NO}_3$ , which has a greater loss rate on the filter, is the most likely reason for our longer filter lifetime, and a general advantage when the system is operating in cold environments. Additionally, aerosol mass loadings may be different in the environments observed in these studies. Better tech-

niques for addressing filtering of the inlet air, and hopefully the ability to remove inlet filters by use of an aerosol separation system, should decrease uncertainties due to inlet losses.

Our system is based upon a continuous wave diode laser, which is smaller and more power efficient than the dye laser system used by Brown *et al.*<sup>12–14</sup> The whole optical system of our instrument is constructed using solid-state components. The price of a cw-CRDS system is significantly cheaper than that of a yttrium–aluminum–garnet (YAG)-pumped dye laser system, and there are no consumables (e.g., dyes, solvents, and flashlamps needed for the YAG-based system). When using cw CRDS, mode matching is an issue, and we have developed techniques to solve these problems. In the future, improvements in the mode matching methods should help in achieving higher data rates, increasing time resolution as well as lowering detection limits. On the other hand, mode matching is adversely affected by vibrations of the cavity and possibly by thermal gradients within the cavity, therefore operating the cw CRDS system is probably going to be more difficult in vibration-rich environments, such as airplanes.

The detection limit of the current system can be compared to that of Brown *et al.*<sup>12–14</sup> The method used by Brown *et al.* is to estimate the detection limit from the variability in the ring-down time, corrected for inlet losses and a theoretical estimate of the zero differencing noise. If we use the same method, we predict a  $2\sigma$  detection limit for  $\text{NO}_3$  at STP of 1.2 pptv in a 25 s average. In the same averaging time, the predicted detection limit for  $\text{N}_2\text{O}_5$  is 1.6 pptv ( $2\sigma$ ). These detection limits are comparable to those of Brown *et al.*, who state 0.5 pptv ( $2\sigma$ ) detection limit for  $\text{NO}_3$  in 5 s using this estimation method.<sup>13</sup> Some of this difference arises from the fact that Brown *et al.*'s base line ring-down time is 50% longer than ours, leading to longer effective path lengths and lower absorption noise. By using times where the  $\text{N}_2\text{O}_5$  signal is zero, we are able to determine actual detection limits including the effect of zero drift and the zeroing difference. Using this data based method, we find that the detection limit is about 50% worse than calculated. We prefer this method of estimation of actual field detection limits. Therefore, we state our detection limit for  $\text{N}_2\text{O}_5$  ( $2\sigma$ ) is 2.4 pptv in a 25 s averaging time. Clearly from the data shown, this detection limit is capable of detection of  $\text{N}_2\text{O}_5$  in ambient air in Fairbanks.

## ACKNOWLEDGMENTS

The author would like to acknowledge the assistance of former group members and visitors Eric Dick, Tomoki Nakayama, Martin King. Funding was provided by a National Science Foundation Grant (CHE-00-94038).

<sup>1</sup>R. P. Wayne, I. Barnes, P. Biggs, J. P. Burrows, C. E. Canosa-Mas, J. Hjorth, G. Le Bras, G. K. Moortgat, D. Perner, G. Poulet, G. Restelli, and H. Sidebottom, *Atmos. Environ., Part A* **25A**, 1 (1991).

<sup>2</sup>F. J. Dentener and P. J. Crutzen, *J. Geophys. Res.* **98**, 7149 (1993).

<sup>3</sup>B. J. Finlayson-Pitts and J. N. Pitts, Jr., *Chemistry of the Upper and Lower Atmosphere* (Academic, San Diego, 2000).

<sup>4</sup>I. Wängberg, T. Eitzkorn, I. Barnes, U. Platt, and K. H. Becker, *J. Phys. Chem. A* **101**, 9694 (1997).

- <sup>5</sup>H. S. Johnston, H. F. Davis, and Y. T. Lee, *J. Phys. Chem.* **100**, 4713 (1996).
- <sup>6</sup>U. Platt, D. Perner, J. Schroeder, C. Kessler, and A. Toennissen, *J. Geophys. Res.* **86**, 11965 (1981).
- <sup>7</sup>F. Heintz, U. Platt, H. Flentje, and R. Dubois, *J. Geophys. Res.* **101**, 22891 (1996).
- <sup>8</sup>U. Platt and F. Heintz, *Isr. J. Chem.* **34**, 289 (1994).
- <sup>9</sup>S. R. Ailwell and R. L. Jones, *J. Geophys. Res.* **103**, 5719 (1998).
- <sup>10</sup>A. R. Weaver, S. Solomon, R. W. Sanders, K. Arapag, and H. L. Miller, *J. Geophys. Res.* **94**, 11041 (1996).
- <sup>11</sup>J. M. C. Plane and C.-F. Nien, *Rev. Sci. Instrum.* **63**, 1867 (1992).
- <sup>12</sup>S. S. Brown, H. Stark, S. J. Ciciora, and A. R. Ravishankara, *Geophys. Res. Lett.* **28**, 3227 (2001).
- <sup>13</sup>S. S. Brown, H. Stark, S. J. Ciciora, R. J. McLaughlin, and A. R. Ravishankara, *Rev. Sci. Instrum.* **73**, 3291 (2002).
- <sup>14</sup>S. S. Brown, H. Stark, and A. R. Ravishankara, *Appl. Phys. B: Lasers Opt.* **75**, 173 (2002).
- <sup>15</sup>M. D. King, E. M. Dick, and W. R. Simpson, *Atmos. Environ.* **34**, 683 (2000).
- <sup>16</sup>S. M. Ball, I. M. Povey, E. G. Norton, and R. L. Jones, *Chem. Phys. Lett.* **342**, 113 (2002).
- <sup>17</sup>B. A. Paldus and R. N. Zare, in *Cavity-Ringdown Spectroscopy: An Ultratrace-Absorption Measurement Technique*, edited by K. W. Busch (American Chemical Society, Washington, DC, 1998), Vol. 720.
- <sup>18</sup>G. Berden, R. Peeters, and G. Meijer, *Int. Rev. Phys. Chem.* **19**, 565 (2000).
- <sup>19</sup>D. B. Atkinson, *Analyst.* **128**, 117 (2003).
- <sup>20</sup>A. O'Keefe and D. A. G. Deacon, *Rev. Sci. Instrum.* **59**, 2544 (1988).
- <sup>21</sup>D. Z. Anderson, J. C. Frisch, and C. S. Masser, *Appl. Opt.* **23**, 1238 (1984).
- <sup>22</sup>K. J. Schulz and W. R. Simpson, *Chem. Phys. Lett.* **297**, 523 (1998).
- <sup>23</sup>D. Romanini, A. A. Kachanov, N. Sadeghi, and F. Stoeckel, *Chem. Phys. Lett.* **264**, 316 (1997).
- <sup>24</sup>B. A. Paldus, C. C. Harb, T. G. Spence, B. Wilke, J. Xie, J. S. Harris, and R. N. Zare, *J. Appl. Phys.* **83**, 3991 (1998).
- <sup>25</sup>B. A. Paldus, J. S. Harris, J. Martin, J. Xie, and R. N. Zare, *J. Appl. Phys.* **82**, 3199 (1997).
- <sup>26</sup>S. P. Sander, *J. Phys. Chem.* **90**, 4135 (1986).
- <sup>27</sup>A. R. Ravishankara and R. L. Mauldin, *J. Geophys. Res.* **91**, 8709 (1986).
- <sup>28</sup>C. A. Cantrell, J. A. Davidson, R. E. Shetter, B. A. Anderson, and J. G. Calvert, *J. Phys. Chem.* **91**, 5858 (1987).
- <sup>29</sup>R. J. Yokelson, J. B. Burkholder, R. W. Fox, R. K. Talukdar, and A. R. Ravishankara, *J. Phys. Chem.* **98**, 114 (1994).
- <sup>30</sup>W. B. DeMore, S. P. Sander, D. M. Golden, R. F. Hampson, M. J. Kurylo, C. J. Howard, A. R. Ravishankara, C. E. Kolb, and M. J. Molina (1997).
- <sup>31</sup>J. B. Burkholder and R. K. Talukdar, *Geophys. Res. Lett.* **21**, 581 (1994).
- <sup>32</sup>S. M. Anderson and K. Mauersberger, *Geophys. Res. Lett.* **19**, 933 (1992).
- <sup>33</sup>W. Schneider, G. K. Moortgat, G. S. Tyndall, and J. P. Burrows, MPI Mainz, Germany, 1986.
- <sup>34</sup>A. C. Eckbreth, *Laser Diagnostics for Combustion Temperature and Species* (Gordon and Breach, Amsterdam, 1996).
- <sup>35</sup>C. E. Canosa-Mas, M. D. King, L. Mcdonnell, and R. P. Wayne, *Phys. Chem. Chem. Phys.* **1**, 2681 (1999).
- <sup>36</sup>J. A. Davidson, A. A. Viggiano, C. J. Howard, L. Dotan, F. C. Fehsenfeld, D. L. Albritton, and E. E. Ferguson, *J. Chem. Phys.* **68**, 2085 (1978).
- <sup>37</sup>H. J. Beine, D. A. Jaffe, J. Herring, J. A. Kelley, T. Krognes, and F. Stordal, *J. Atmos. Chem.* **27**, 127 (1997).
- <sup>38</sup>H. J. Beine, Ph.D. thesis, University of Alaska, Fairbanks, 1996.